Transparent Ultra-Long-Haul DWDM Networks With "Broadcast-and-Select" OADM/OXC Architecture

Michael Vasilyev, *Member, IEEE, Member, OSA*, Ioannis Tomkos, *Member, IEEE*, Manjusha Mehendale, June-Koo Rhee, *Member, IEEE*, Andrey Kobyakov, *Member, IEEE*, Mahesh Ajgaonkar, Sergio Tsuda, and Manish Sharma, *Member, IEEE*

***Abstract*—We describe an experimental realization of ultra-long-haul (ULH) networks with dynamically reconfigurable transparent optical add–drop multiplexers (OADMs) and optical cross-connects (OXCs). A simple new approach to dispersion management in ULH dense-wavelength-division-multiplexing (DWDM) transparent optical networks is proposed and implemented, which enables excellent transmission performance while avoiding dispersion compensation on a connection-by-connection basis. We demonstrate "broadcast-and-select" node architectures that take full advantage of this method. Our implementation of signal leveling ensures minimum variations of path-averaged power among the wavelength-division-multiplexing (WDM) channels between the dynamic gain-equalizing nodes and results in uniform nonlinear and spontaneous-emission penalties across the WDM spectrum. We achieve 80 $\times$ 10.7-Gb/s DWDM networking over 4160 km (52 spans $\times$ 80 km each) of all-Raman-amplified symmetric dispersion-managed fiber and 13 concatenated OADMs or 320 $\times$ 320 wavelength-port OXCs with 320-km node spacing. The WDM channels use 50-GHz grid in C band and the simple nonreturn-to-zero (NRZ) modulation format. The measured Q values exhibit more than a 1.8-dB margin over the forward-error correction threshold for 10^{-15} bit-error-rate operation. We compare these results with point-to-point transmission of 80 $\times$ 10-Gb/s NRZ WDM signals over 4160 km without OADM/OXC and provide detailed characterization of penalties due to optical signal-to-noise-ratio degradation, filter concatenation, and crosstalk.**

***Index Terms*—Add–drop multiplexer, dispersion management, optical communication, optical cross-connect (OXC), Raman amplification, transparent optical networks.**

I. Introduction

TRANSPARENT ultra-long-haul (ULH) network systems have gained strong importance in the past few years, as the longer transparent reach distance of optical circuit connection promises network cost reduction through elimination of costly optical-to-electrical-to-optical (O/E/O) data regenerators. In a legacy opaque dense-wavelength-division-multiplexing (DWDM) network model, all DWDM channels are O/E/O-regenerated at every add–drop or cross-connect node, which leads to excessive network cost. According to recent studies of the U.S. traffic demands and network topology, the average connection distance is about 2700 km, and the average node spacing is only 600 km [1], [2]. Under such conditions, it is evident that for a cost-effective network implementation, most of the traffic should pass transparently through the network nodes. In fact, only approximately 25% of the traffic on average is dropped to and added from the node in typical nationwide network systems of the North America region. In order to save the O/E/O cost of the remaining 75% of the traffic that passes the node, networks supporting ULH transmissions with reach in excess of 2700 km are required. Recent progress in transmission technologies now enables point-to-point terrestrial ULH transmission up to 8000 km without O/E/O regeneration, by use of combinations of forward-error correction (FEC), new data modulation formats, and Raman amplification, as well as new types of fibers and dispersion compensators (DCs) (for review of recent transmission experiments, see, e.g., [3]). In order to make use of the full benefit of ULH transmission technologies, however, optical add–drop multiplexers (OADMs) need to be deployed to allow optical pass-through as well as partial add–drop for the local traffic. Because of the dynamics and growth of the network, reconfigurability of OADMs is an important function.

Further flexibility and cost reduction can be achieved by eliminating the electronic cross-connect fabric and replacing it with reconfigurable transparent optical cross-connect (OXC). OXCs cross-connect traffic from various directions, support network restoration after network failure, and dynamically provision the network traffic demand. The increasing interest in OXCs capable of ULH transparent networking comes from the growing need for a cost-effective interconnection of data traffic originating from major cities.

While ULH point-to-point transmission experiments have reached terabit capacities over many thousands of kilometers, only a few of them include network elements along the signal path [2], [4]–[7]. We have recently presented the first results on 80 $\times$ 10.7-Gb/s OADM and OXC networks with 4160-km reach and 320-km distance between the network nodes [6], [7]. In this paper, we give the full account of our experiments on ULH networking and discuss in depth the innovative approaches that enabled them. A special consideration is given to

Manuscript received December 12, 2002; revised July 3, 2003.

M. Vasilyev was with Corning Incorporated, Somerset, NJ 08873 USA. He is now with the Department of Electrical Engineering, University of Texas, Arlington, TX 76019 USA (e-mail: vasilyev@uta.edu).

I. Tomkos was with Corning Incorporated, Somerset, NJ 08873 USA. He is now with Athens Information Technology–Center of Excellence for Research and Graduate Education, Peania 19002, Greece.

M. Mehendale was with Corning Incorporated, Somerset, NJ 08873 USA. She is now with Center for Ultrafast Laser Applications, Princeton University, Princeton, NJ 08544 USA.

J.-K. Rhee was with Corning Incorporated, Somerset, NJ 08873 USA. He is now with Samsung Advanced Institute of Technology, Korea.

A. Kobyakov, M. Ajgaonkar, S. Tsuda, and M. Sharma are with Corning Incorporated, Corning, NY 14831 USA.

Digital Object Identifier 10.1109/JLT.2003.819557

the issue of designing the optimum dispersion map that enables best network performance at low cost. We discuss the choice of appropriate pre-emphasis to obtain adequate performance across the entire wavelength-division-multiplexing (WDM) spectrum. We provide a detailed performance comparison of the point-to-point ULH transmission, OADM, and OXC ULH networks. Our system performance measurements reflect the impacts of both transmission and networking impairments, including amplified spontaneous emission (ASE) and double-Rayleigh backscattering (DRBS) noise accumulation, filter concatenation, dispersion, fiber nonlinearity, polarization-dependent loss (PDL), and polarization-mode dispersion (PMD). We fully characterize the impact of filter concatenation, as well as single-term and 24-term crosstalks on the performance of the ULH network.

The key enabling technologies in our experiments are "broadcast-and-select" OADM and OXC architectures [8], [9], symmetric dispersion-managed fiber optimized for Raman amplification [10], [11], novel spectral pre-emphasis and dispersion mapping approaches, as well as the excellent crosstalk, insertion loss, and filter concatenation performance of Corning® Wavelength Blocker [12], performing both the wavelength blocking and (in OADM experiments) leveling functions.

The paper is structured as follows. In Section II, we introduce the broadcast-and-select architectures for OADM and OXC. Section III discusses the issues of dispersion map optimization in the network context. Section IV reviews the benefits of symmetric dispersion-managed fiber employed in our experiments. Section V describes our approach to dynamic spectral equalization and optimum signal pre-emphasis. Section VI presents our results for point-to-point ULH transmission, which serve as the baseline for comparison to our networking results. Sections VII and VIII review our results for OADM and OXC networking, respectively. The last section summarizes the results.

II. Broadcast-and-Select Node Architecture

The broadcast-and-select (B&S) architecture represents an emerging alternative to the conventional parallel OADM approaches (e.g., wavelength-layered and fully connected switch fabric designs) and is particularly well suited for ULH applications, where each signal travels through multiple OADM nodes [9]. B&S OADMs exhibit exceptionally low loss for pass-through channels, achieving greater distances without regeneration, and have built-in spectral equalization capability. In networks with large fraction of express traffic, they offer lower first-installed cost by integrating the multiplexing, switching, and equalization functions in fewer components, and scale more cost-effectively because wavelength access can be added as needed.

The B&S OADM architecture used in our experiments consists of a 1×1 wavelength-selective switch, or wavelength blocker (WB), in combination with 1×2 power splitters/combiners to perform traffic add–drop and proper amplification to compensate for OADM losses. In this architecture, shown in Fig. 1, all incoming traffic is split into two paths for drop and pass-through. In the drop path, the dropped traffic is selected by a combination of a power splitter ($1 \times N$, where N is the number of simultaneously accessible DWDM channels) and tunable filters. In the pass-through path, the WB blocks the dropped channels, and the corresponding blank channel slots are available for the new channels arriving from the add path. The add path may consist of N tunable transmitters and an $N \times 1$ power combiner. An erbium-doped fiber amplifier (EDFA) is used to compensate for losses in the add path (when high add–drop ratio and colorless multiplexer are used), and the amplifier noise in the empty channel slots is removed by an ASE filter (e.g., another WB). Both WBs in this architecture can block selected channels and simultaneously level the power for the pass-through or added channels. EDFAs are placed at the input and the output of the OADM to compensate for OADM losses.

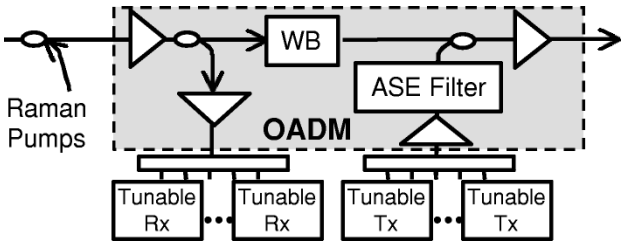

Fig. 1. B&S OADM architecture.

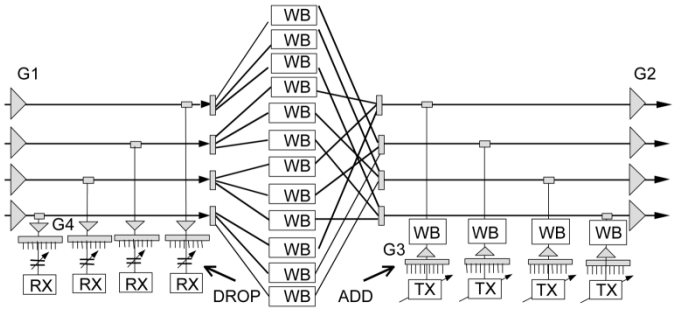

Fig. 2. B&S OXC architecture.

The B&S architecture also enables the design of transparent OXCs. To demonstrate this, we consider the case of an OXC capable of handling 320×320 wavelength ports (4×4 physical ports), which we realize in our experiments discussed in Section VIII. In this particular design, we rule out the loop-back connection requirement, that is, we do not provide any connection between the incoming and outgoing fibers of the same cable link. The resulting B&S OXC consists of 1×1 WBs in combination with power splitters/combiners to perform traffic cross-connection–add–drop, and proper amplification to compensate for fixed OXC losses (Fig. 2). All incoming traffic at an input port of the OXC is split into two paths for local drop and cross-connect traffic. In the drop path, the dropped traffic is selected by a combination of a power splitter ($1 \times N$, where N is the number of simultaneously accessible DWDM channels) and tunable filters. In the cross-connect path, the signals are split and broadcast by 1×3 power dividers to three WBs. These WBs block the paths for the channels designated for local add–drop and provide every remaining channel of every input fiber with an individual connection to its corresponding single output fiber of destination. Since the dropped traffic is blocked by the WBs, the available channel slots can be filled by signals coming from the

add path. At each OXC output port, a 3×1 coupler combines the channels coming from three WBs connected to different OXC input ports. An add path consists of N tunable transmitters and an $N \times 1$ power combiner to provide the added traffic. An EDFA is employed to compensate for losses in the add path if a high percentage of the traffic is added/dropped and a colorless multiplexer is used. The WDM comb is then filtered by another WB, which reduces the noise level in the channel slots corresponding to the pass-through traffic. EDFAs are placed at selected points along the signal path in the OXC to maintain a proper power level for the dropped and pass-through traffic.

The WB is a critical element in both OADM and OXC B&S architectures. In the B&S experiments described in this paper (Sections VII and VIII), we employ Corning® Wavelength Blocker. In this device, the WDM input is spectrally decomposed in free space, where a liquid-crystal-based spatial light modulator independently attenuates individual channels, which are recombined again at the output. The WB has an insertion loss of < 6 dB, a blocking extinction ratio (crosstalk) of > 40 dB, an equalization (leveling) range of 0–20 dB, and a polarization-dependent loss of < 0.3 dB and is capable of handling more than 80 channels at 50-GHz spacing. The transition time from minimum insertion loss ("open") to fully blocking state ("closed") is < 2 ms, whereas the transition time from "closed" to "open" is < 35 ms. In our experiments, the WB is controlled by a laboratory computer through a standard electrical interface.

III. Dispersion Management

This section describes a novel dispersion management technique that can be used in 10-Gb/s transparent ULH optical networks. It is simple and cost-effective to implement and provides superior performance by eliminating the resonant build-up of nonlinear penalties. We will show below that this technique is particularly easy to use in B&S OADM and OXC networks, where it needs only one broad-band dispersion compensator per add or drop port carrying multiple channels, in contrast with other architectures requiring separate DCs for every added or dropped channel.

Success of ULH DWDM transmission critically depends on the accurate dispersion management. In particular, for 10-Gb/s systems, high local dispersion is required to avoid cross-channel impairments, such as four-wave mixing (FWM) and cross-phase modulation (XPM). At the same time, the net end-to-end accumulated dispersion must be low enough to avoid linear signal distortion and conversion of the nonlinear phase impairments (XPM and self-phase modulation) into the amplitude ones. Hence, the dispersion maps for ULH transmission usually require dispersion compensation after every amplifier span. This can be done by either using dispersion slope-compensating modules at the amplifier sites or by employing dispersion-managed fiber as the transmission medium. Best transmission results are obtained when such per-span dispersion compensation does not completely compensate for 100% of the dispersion of transmission fiber in the span. In other words, slight per-span under-compensation is desired for optimum performance [13]. This under-compensation helps to avoid the resonant accumulation of FWM and XPM impairments. The build-up of the residual dispersion in ULH systems requires the use of some pre- and or postcompensation at the terminals. While such dispersion maps are well known and have been studied extensively for point-to-point transmission systems, little consideration has been given as to how they may be adapted for use in transparent ULH optical networks.

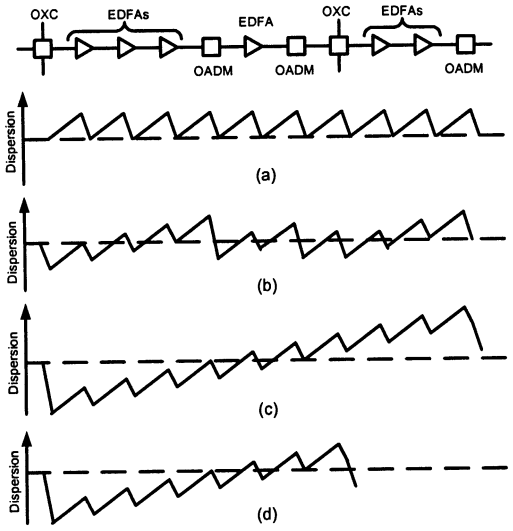

Fig. 3. Dispersion maps for transparent networks: (a) resonant map with zero accumulated dispersion per amplifier span, (b) resonant map with zero accumulated dispersion per optical multiplex section, (c) proposed dispersion map (longest path), and (d) proposed dispersion map (short path).

Three different potential dispersion management techniques can be envisioned for use in transparent optical networks and are illustrated in Fig. 3. Fig. 3(a) shows the simplest solution. Here, the dispersion of each fiber span is fully compensated at each EDFA or node site. This brings the dispersion of each span to zero, and hence, the total accumulated dispersion between any two points in the network will be zero. This approach is likely to avoid the need for any pre- or postcompensation, and all paths would see zero accumulated dispersion. However, such a dispersion map is likely to result in poor transmission performance due to the resonant build-up of cross-channel impairments (FWM and XPM) from each span.

The transmission performance of this scheme can be improved if we choose to under-compensate each amplifier span and use pre- and post- compensation at OADM and OXC sites to ensure zero accumulated dispersion between any two adjacent nodes in the network [14]. This approach is shown in Fig. 3(b). Effectively, the dispersion is managed on an optical-multiplex-section basis. Since this map is less resonant than the first approach, we expect an improvement in transmission performance. However, performance is likely to degrade when many nodes are placed close together, since the dispersion map becomes a lot more resonant.

The best performance can be obtained by using our proposed solution, which is a completely nonresonant dispersion map, as shown in Fig. 3(c). This will require the use of pre- and/or post-compensators to reduce the accumulated dispersion of each channel, and clearly, the amount of accumulated dispersion will vary on a channel-by-channel basis, since each channel could

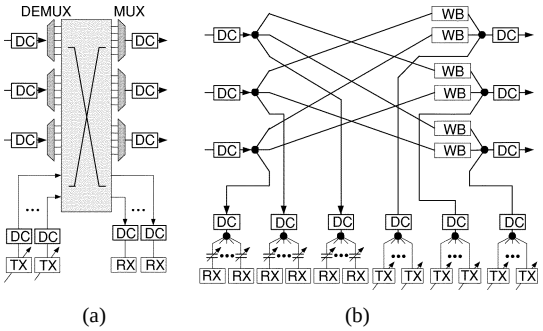

Fig. 4. Placement of DC modules in OXCs/OADMs: (a) traditional three-dimensional microelectromechanical (MEMS)-based architecture and (b) broadcast-and-select architecture.

potentially travel a completely different path length. While this would indicate that some kind of adjustable or settable per-channel dispersion compensator is needed to obtain the correct amount of dispersion compensation for each channel, we propose the use of a uniform amount of pre- and/or postcompensation for all channels *irrespective of path length*. By optimizing the amount of pre- and postcompensation for the longest path length to be supported in the network, we can ensure that all shorter paths see adequate performance [Fig. 3(d)]. *These shorter paths incur smaller amounts of signal degradation due to ASE and nonlinearites, and this margin enables better tolerance for the cumulative residual dispersion penalty*. Although the performance of these shorter paths could be improved by re-adjusting the amount of pre- and postcompensation, even their non-optimum performance can still be shown to be adequate and better than the performance at the maximum path length. This technique requires that the total amount of pre- and postcompensation be chosen such that sufficient performance can be obtained in the back-to-back cases, where almost no nonlinear or optical signal-to-noise ratio (OSNR) impairments are present and the performance is mostly dispersion limited due to the pre- and postcompensation [15], [16]. Even with -1000-ps/nm pre-compensation, the back-to-back 10-Gb/s performance is usually adequate because of high initial OSNR. While the exact dispersion map details (e.g., amounts of pre-, post-, and per-span under-compensation) depend on the system reach, span length, modulation format, etc., some rules of thumb are usually common for 10-Gb/s ULH links: using 20–100-ps/nm per-span under-compensation (to avoid the resonance) and not exceeding ~ 1500 ps/nm (for NRZ; RZ can tolerate in excess of 2000 ps/nm) in absolute value of accumulated dispersion before or after any span.

In addition to enabling superior transmission performance, the proposed dispersion management technique is also highly compatible with B&S node architectures discussed in the previous section. As shown in Fig. 4(a), traditional OXC/OADM architectures can support resonant dispersion maps very well, since DCs can easily be placed on the ingress and egress ports of the node. However, in order to apply pre- and/or postcompensation to channels as they enter or leave the network, single-channel dispersion compensators are required. This typically prohibitively expensive dispersion management solution can be avoided by using B&S node architectures [Fig. 4(b)]. The B&S OADM/OXC nodes operate by passively broadcasting all incoming signals to all output ports and using WBs to control which channels are coupled through to which output port. Since all channels being added to a particular outgoing fiber are first multiplexed together onto a single fiber, this provides a convenient place to simultaneously pre-compensate all channels by using only a single dispersion compensator. Dropped channels can be post-compensated in a similar manner by using only a single dispersion compensator per egress port.

The exact dispersion maps shown in Fig. 3 represent the spans made of a single fiber type (e.g., standard single-mode fiber or nonzero-dispersion-shifted (NZ-DSF) fiber) and utilize DC modules at the amplifier sites. However, the same concepts of resonant and nonresonant mapping and our proposed dispersion management scheme apply to dispersion-managed fiber spans, where the only difference is that all or most of the fiber dispersion is compensated within the span itself, thereby eliminating the need for the amplifier-site DCs. In addition to similar network-related advantages of Fig. 3(c) and (c)-like dispersion maps for both single and dispersion-managed fibers, the latter offers further point-to-point transmission performance improvement, owing to optimized dispersion management within each span, as discussed in Section IV.

It is worth mentioning that the proposed dispersion map makes it easy to extend the B&S OADM/OXC approach to hubbing systems with long branch links. Since the dispersion map is optimized for the longest path (including branch reach), and the OSNR is budgeted to allow longest path with every channel added and dropped at some points, both branch-link and locally added/dropped channels will perform adequately.

The proposed simple and cost-effective dispersion map that employs the same fixed amount of pre-compensation for every transmitter in the network is one of the key enablers of our experiments described in Sections VI–VIII.

IV. Symmetric Dispersion-Managed Fiber

As we have discussed in the previous section, the accurate compensation of the dispersion and dispersion slope is imperative for ULH systems. This is most frequently achieved by using short pieces of dispersion-compensating fiber at the amplifier sites. Most recently, however, dispersion-managed-fiber (DMF) spans that comprise a large-effective-area positive-dispersion fiber ($+$D) and a slope-matching reverse-dispersion fiber ($-$D) have gained popularity, in particular, in submarine systems. With their high absolute values of local fiber dispersion, which is important for FWM and XPM reduction, and the ability to very precisely compensate the dispersion across the entire WDM signal spectrum, DMFs have significant advantages over standard single-mode and NZ-DSF. In particular, they create a potential for replacement of the return-to-zero (RZ) modulation format with the less expensive nonreturn-to-zero (NRZ) in transatlantic transmission [17]. In addition, the reduction of the mid-stage loss requirement of an EDFA with the removal of the dispersion compensation fiber also allows for a reduction in the effective amplifier noise figure. DMFs provide a further benefit of stability of the compensation since both $+$D and $-$D fibers are exposed to the same outside plant environment and have opposite signs of temperature-induced dispersion variations [18].

Deployment of DMF in terrestrial systems, where the spans are longer, frequently requires from DMF the compatibility with distributed Raman amplification. Typically, the $-$D fiber has a smaller effective area than the $+$D fiber, and hence, placing the $-$D fiber at the end of the span ($+$D/$-$D configuration, typical for submarine experiments) results in most of the Raman gain being generated in the small-effective-area $-$D fiber. This makes $+$D/$-$D DMF highly prone to Raman-induced DRBS, which is inversely proportional to the square of effective area and capable of causing substantial system penalties. A symmetric configuration of DMF has been recently introduced [10], [19], where the $-$D section is positioned between two approximately equal sections of the $+$D fiber. In this DMF design, only a fraction of the total Raman gain is generated in $-$D fiber, hence, the DRBS is significantly reduced. In addition, with symmetric DMF, the pump intensity in the $-$D fiber section is high enough to produce significant Raman gain early in the span. As a result, the signal power in the symmetric configuration is never attenuated as deeply as that in the asymmetric configuration, leading to much better Raman noise figure performance of the symmetric design. In addition to its excellent noise properties, the symmetric arrangement may also cancel certain types of nonlinear penalties [11], [20], [21]. All these advantages have made the symmetric DMF the preferred fiber choice for high-capacity ULH DWDM transmission experiments [22]–[25].

V. Dynamic Gain Equalization and Optimized Pre-Emphasis

Residual spectral ripple, contributed by amplifiers and WDM components, accumulates over many spans and severely degrades ULH DWDM systems, leading to OSNR reduction for the channels in the gain ripple minima and to nonlinear penalties for the channels in the ripple maxima. In addition, a ripple with sharp spectral features also subjects the channels in the ripple minima to interchannel penalties from their powerful neighbors. These problems can be partially mitigated by dynamic gain-flattening filters (DGFFs) cleaning up the ripple after every few spans. While DGFF flattens the spectrum, it cannot reverse the signal impairments already incurred between the clean-ups. The resulting uneven system performance among the WDM channels needs to be flattened by appropriate pre-emphasis at every DGFF location.

It is well known that the pre-emphasis producing *flat OSNR* before the next clean-up outperforms that producing *flat spectrum* before the clean-up [26]–[28]. However, flat-OSNR pre-emphasis does not necessarily guarantee similar nonlinear penalties (and, therefore, similar Q values) among the channels, since some channels will require considerably higher powers than other channels in order to obtain the same OSNR. In addition, it requires OSNR monitoring, which is not an easy task in high-spectral-efficiency DWDM systems, where the spectra of neighboring channels overlap and hide the ASE noise floor. In addition, in a transmission link with many DGFFs, optimization of DGFF settings using only terminal OSNR monitoring becomes complicated, whereas monitoring small OSNR decrements at each DGFF location is costly and inaccurate. For nonlinearity-limited systems, a pre-emphasis method based on Q measurements has been proposed [29].

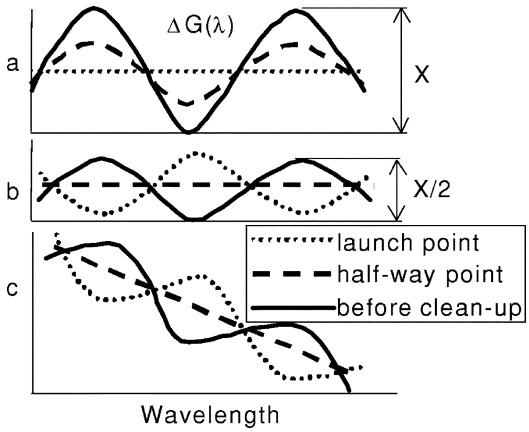

Fig. 5. Signal spectra for three pre-emphasis scenarios: (a) launched spectrum is flat; (b) spectrum at halfway point is flat; and (c) tilted straight-line spectrum at halfway point.

In our experiments throughout this paper, we employ another method of pre-emphasis, based on channel power, rather than OSNR or Q measurements, which reduces the variations of path-averaged power among the channels. The practical implementation of our method is very simple and inexpensive, as it does not require either the estimation of the ASE noise floor between the channels or high-speed signal detection as OSNR- and Q-monitoring, respectively, do. This makes it easy to use the proposed pre-emphasis with channel-power monitoring at every DGFF location. As shown in Sections VI–VIII, despite its simplicity, this method results in relatively uniform OSNR and Q performance among all channels, as it balances the two dominant impairments in ULH links, the ASE and nonlinearity.

Let us consider the case of launching a flat spectrum into the first span after a clean-up. Let us assume that the last span's output before the next DGFF clean-up has a shape given by $G(\lambda) = G_{\text{average}} + \Delta G(\lambda)$ (in decibels), where $\max(\Delta G) - \min(\Delta G) = X$ dB ripple [Fig. 5(a)]. If we pre-emphasize the launch spectrum into the first span by the amount of $-\Delta G(\lambda)/2$, the spectrum becomes flat halfway between the DGFF clean-ups and has the same $X/2$-dB ripple before the first span and after the last span. This reduces the maximum power excursion among the channels to half of the original gain ripple, thereby improving both nonlinear penalties and minimum OSNR [Fig. 5(b)]. If, in addition to gain ripple, there is also a noise-figure tilt typical to Raman-assisted systems, the launch spectrum into the first span can be tilted [Fig. 5(c)] until the OSNRs after the last span are equalized within a fraction of a decibel. Since, unlike the gain ripple, the noise-figure tilt is deterministic and systematic, this step involving OSNR measurements needs to be performed only once during the system design or installation. For DWDM systems with channel add–drop capabilities, the tilt can be dynamically reset according to empirically obtained channel-load dependence. Thus, in our pre-emphasis method, the spectrum halfway between two consecutive DGFFs is a straight line with a slope determined by the required tilt (for 1–2-dB tilt, an approximately straight line appears on both linear and logarithmic scales).

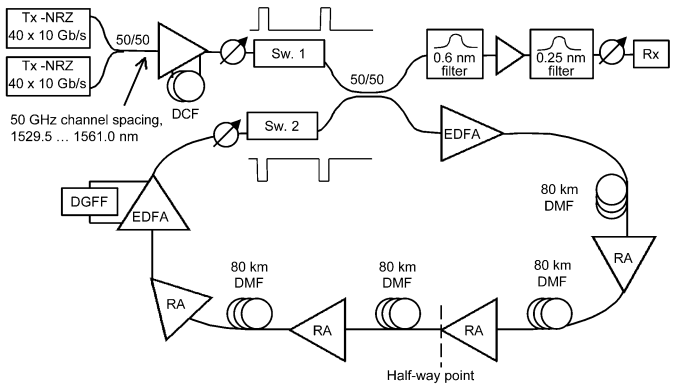

Fig. 6. Experimental setup.

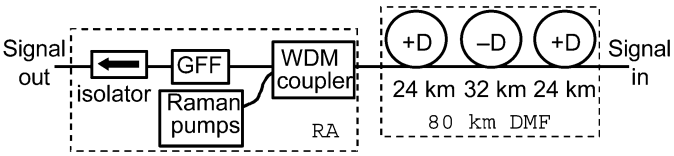

Fig. 7. RA with one span of DMF.

In the ULH network, it is cost effective to combine the functions of gain equalization (leveling) and B&S blocking in a single device, such as WB. This tightens the requirements on the extinction ratio of the WB, which now becomes the sum of the blocking crosstalk and node leveling specifications (on logarithmic scale).

VI. Point-to-Point Ultra-Long-Haul Transmission Experiments

In order to understand the relative impact of the network-specific impairments, we have first performed point-to-point transmission experiments that provide us with an important performance baseline [22].

The schematic of our experimental recirculating-loop setup is shown in Fig. 6. We obtain 80 channels spaced by 50 GHz (1529.55...1561.01 nm) by interleaving two sets of 40 DFB lasers, each having channel spacing of 100 GHz. Each set of lasers is multiplexed with arrayed-waveguide gratings and modulated with a $2^{31}-1$ 10-Gb/s pseudorandom bit sequence (PRBS) by a lithium niobate Mach–Zehnder modulator.

The recirculating loop consists of four 80–km spans of symmetric DMF, each comprising 32 km of the $-$D fiber positioned between two 24-km sections of the $+$D fiber (see Fig. 7). The average per-span residual dispersion is around 28 ps/nm, making the total dispersion equal to (110 ± 8) ps/nm per loop across the entire C band. All spans are made transparent by using distributed Raman amplification. This is achieved by pumping the spans in the backward direction with three pairs of Raman pumps (three wavelengths, two polarizations). The pump powers are adjusted to achieve the transparency with minimum gain ripple in the spectrum. Each Raman amplifier (RA) also includes a fixed gain-flattening filter (GFF), as shown in Fig. 7. The average Raman gain to compensate for losses of the fiber, splices, connectors, Raman WDM coupler, GFF, and an isolator is 20.5 dB.

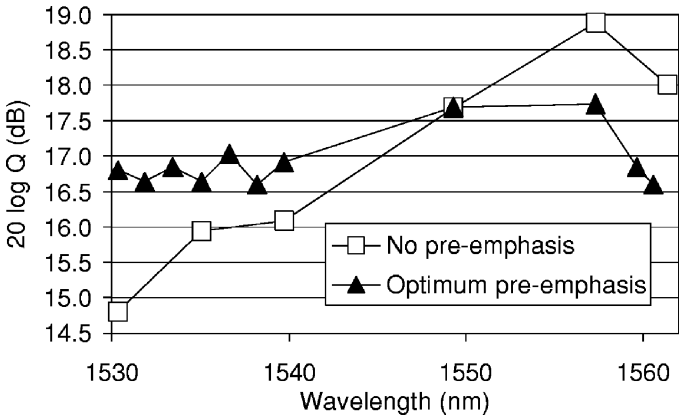

Fig. 8. Q factor of selected channels after 2240 km.

We minimize the accumulation of the residual gain ripple by employing a DGFF positioned in the mid-stage of the EDFA at the end of each loop (every 320 km). This amplifier and a second single-stage EDFA are used to compensate for the DGFF's and loop-specific losses. The smooth character of the EDFA and Raman gain ripple allows a wide choice of DGFF technologies without stringent requirements of high extinction ratio and independent attenuation of individual channels. In our experiment, we employ a dynamic gain equalizer (DGE) that is based on diffractive MEMS technology, has an insertion loss of 4.5 dB, an attenuation range up to 15 dB, a response time of 50 μs, and a polarization loss of < 0.3 dB and is capable of equalizing the ripple after each loop to a small fraction of a decibel. The average launch power is about -6.8 dBm per channel. After 13 circulations corresponding to transmission over 4160 km, a tunable optical bandpass filter with the full-width at half-maximum of 0.25 nm at the receiver's pre-amplifier selects the channel to be measured. For 4160-km transmission, the best performance has been found for uniform pre-compensation of all channels by -986 ps/ nm and no dispersion postcompensation.

We illustrate the pre-emphasis method of Section V by transmission of 40×10–Gb/s NRZ WDM signals (one 40-channel set of 100-GHz-spaced sources is turned off) over 2240 km, with pre- and postcompensation optimized for that reach. Fig. 8 shows Q measured at the receiver for selected channels across the C band. When the launched spectrum is flat, 3.3–dB OSNR and 4.1–dB Q ripples (open squares) are observed. 2.9-dB OSNR and 3-dB Q ripples are measured when the spectrum halfway between DGFFs (160 km) is flat. Finally, when the spectrum is launched according to the optimum pre-emphasis method described in Section V, so that it is flat with 2-dB tilt at the halfway point in the loop, the OSNR has only a 1.5-dB ripple, and the Q ripple is minimized to 1.1 dB (solid triangles in Fig. 8). This method is utilized also in 80-channel transmission over 4160 km.

The spectrum after 4160 km when all 80 channels are turned on is shown in Fig. 9. It exhibits a maximum ripple of 4.3 dB, which also includes the contribution of the 2-dB spectral tilt. The transmission performance was characterized by measuring the bit-error rate (BER) for each channel. The corresponding Q factors and OSNRs are shown in Fig. 10. The worst measured Q across the C-band spectrum is 15.6 dB ($\mathrm{BER} = 8 \times 10^{-10}$).

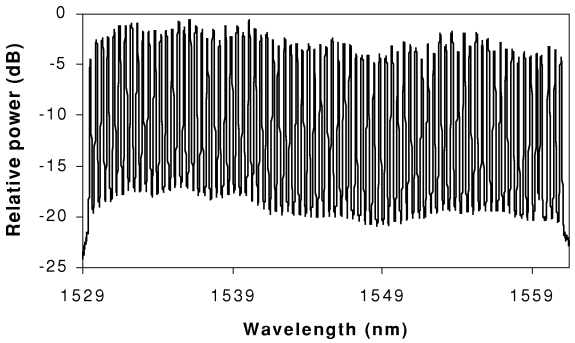

Fig. 9. 80-channel spectrum after 4160 km.

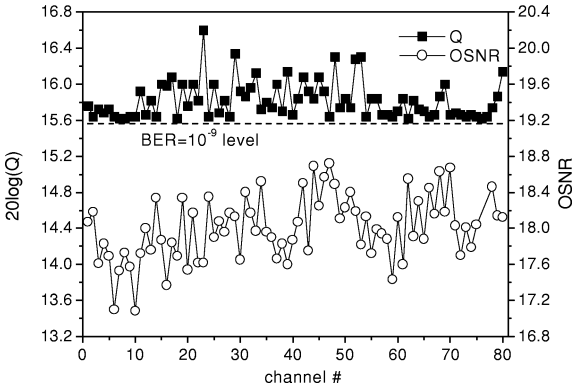

Fig. 10. Q and OSNR for all 80 channels after 4160-km transmission.

The Q and OSNR are reasonably flat, with the average OSNR of 18.0 dB. The minimum OSNR is 17.1 dB for channel 10 (1533.03 nm).

To summarize this section, we have shown that the symmetrically configured ($+$D/$-$D/$+$D) dispersion-managed fiber and dynamic gain equalization with optimum pre-emphasis enable the use of the NRZ modulation format to achieve an error-free ($\mathrm{BER} < 10^{-9}$) 4160-km transmission with a fully populated C-band 50-GHz channel grid in a terrestrial (52 spans $\times$ 80 km each) 80 $\times$ 10-Gb/s all-distributed Raman system without FEC. This produces a significant performance margin to be used for adding the network functionality to our setup, as described in Sections VII and VIII.

VII. Ultra-Long-Haul OADM Networking

This section describes a transport study of the ULH network with fully functional reconfigurable OADMs. The OADMs are based on the B&S architecture, enabled by a WB (Corning® Wavelength Blocker) [9], [12]. The transmission link is the same as that in Section VI, but with OADM positioned at the end of every 320-km loop. The DGFF is removed, as the WB performs the signal leveling as well as wavelength blocking. This system performance study takes into account the impact of both transmission and networking impairments, including the ASE and DRBS noises, filter concatenation, dispersion, fiber nonlinearity, crosstalk, and PDL/PMD.

Using a recirculating-loop setup, we emulate the network model shown in Fig. 11. We assume that 80 channels are added at the first OADM. The 80 channels propagate over 1600 km of fiber (passing through four OADMs), and at the

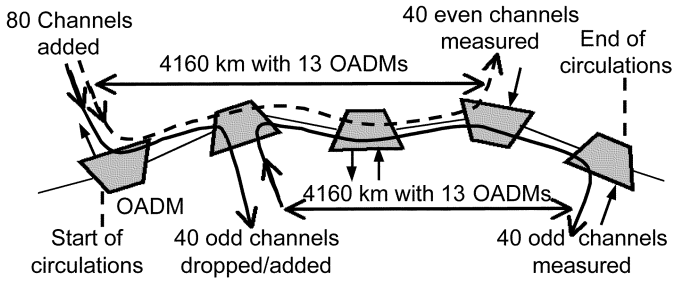

Fig. 11. Network model realized in our recirculating-loop testbed.

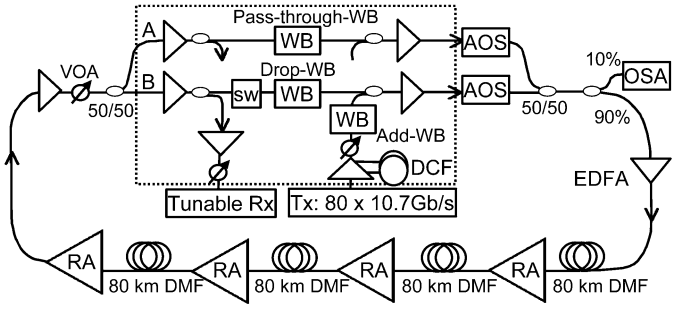

Fig. 12. Schematic of experimental setup.

sixth OADM, 50% of the traffic (odd-numbered channels) is dropped. The OADM adds new traffic at the odd-numbered channels so that a total of 80 WDM channels are sent to the next spans. Fig. 12 shows a schematic of the recirculating-loop setup used in our experiments. The 80 DWDM channels (1530.33 nm . . . 1561.82 nm) are obtained by interleaving two sets of 40 channels, each with 100-GHz channel spacing. A $LiNbO_3$ Mach–Zehnder modulator is used to encode $2^{31}-1$, 10.664-Gb/s NRZ PRBS data on each set of 40 channels. An EDFA is used to amplify the DWDM signals that are fed into the add path of the OADM. Dispersion-compensating fiber (DCF) is placed in the mid-stage of the EDFA to pre-compensate the signals by -986 ps/nm and -1315 ps/nm for transmission over 4160 km and 8000 km, respectively. No postcompensation is used in the drop path for the reach of 4160 km, while for the 8000-km reach, we use –820-ps/nm postcompensation. An EDFA is used before the first span to compensate for losses specific to the loop architecture (i.e., losses from the acoustooptic switches (AOS) and the 3-dB coupler). The average launch power per channel in each fiber span is -6.8 dBm. After passing through the spans, the signals are fed to the OADM (dotted line in Fig. 12). In the drop path of the OADM, they are demultiplexed, pre-amplified, selected by a bandpass filter, and sent to a receiver.

For demonstration purposes only, we implement two OADMs in separate optical paths in our loop experiment (see Fig. 12). The top path (A) is used for the traffic passing through the OADM. The bottom path (B) is used for adding and dropping traffic from the loop. The amplifier at the input of the OADM is placed to accommodate the 3-dB loss of the coupler that splits the signals in the two paths, without introducing OSNR degradation that would not be present in a real OADM design. For the pass-through traffic, the accumulation of gain ripple at the end of the loop is compensated by the "pass-through" WB. This gain

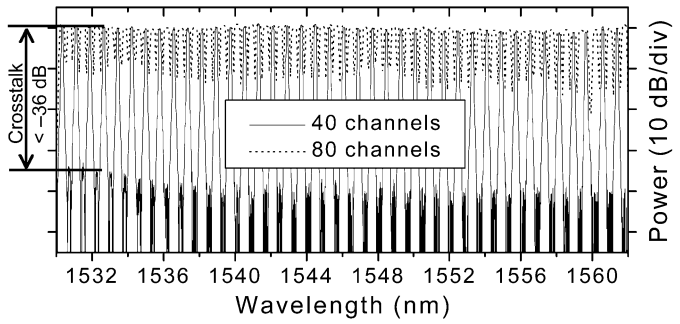

Fig. 13. Spectra at the WB output with and without blocking of every other channel. Resolution bandwidth of optical spectrum analyzer is 0.12 nm.

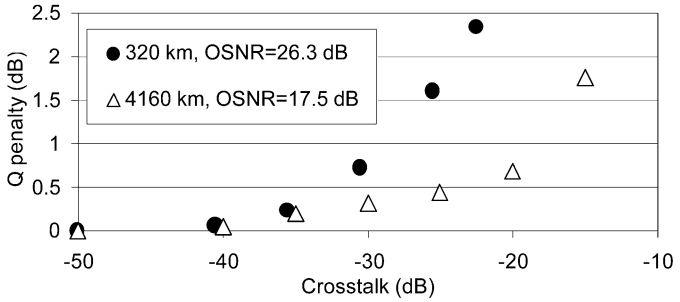

Fig. 14. Crosstalk penalty for channel 25 (1539.77 nm) after 320 km and 4160 km.

equalization and the corresponding pre-emphasis by the "add" WB, following the technique outlined in Sections V and VI, result in relatively small 1.9-dB OSNR ripple and in maximization of the worst Q factors of the received signals. The AOSs, as well as the "drop" and "add" WBs, are dynamically reconfigured to enable loading of the loop with traffic, circulation of signals in the loop, and add–drop functionality after the first five loops. Initially, the loop is loaded with 80 channels through the "add" WB. During the loading time, the light in the bottom path B is blocked by fast mechanical switch "sw." The channels circulate for five loops using the OADM in the top path A with the "pass-through" WB (AOS is "ON" in the top path A and "OFF" in bottom path B). After five loops, the AOS in the bottom path B becomes "ON, " and the AOS in the top path A becomes "OFF," thereby redirecting the signals to the bottom path B. At that point, the 40 odd channels are blocked by the "drop" WB and are added by the "add" WB. Then, the AOSs are reconfigured again, and the signals circulate through the top path A.

The optical spectra at the output of the WB in the OADM are shown in Fig. 13, with either all channels passing through or 40 channels being blocked. The crosstalk performance of the OADM that performs simultaneous blocking and power leveling (3.5–4.5 dB) is greater than 36 dB. The measured polarization-averaged Q penalty due to single-term crosstalk is shown in Fig. 14 for two propagation distances. As expected, because of the lower OSNR, the Q penalty after 4160 km is less than that after 320 km for the same crosstalk level. Table I and Figs. 15 and 16 show the measured OSNR and Q data ($Q[\mathrm{dB}] = 20\log Q_{\mathrm{linear}}$) for three different system configurations. First, solid circles show the 80-channel results from Fig. 10, obtained from a 10-Gb/s 4160-km transmission test without any OADM, but with leveling performed by a DGFF at an EDFA mid-stage. Second, open diamonds in Figs. 15 and 16 show the 10.66-Gb/s performance with all 80 channels passing through 13 concatenated OADMs without introducing any crosstalk (0% add–drop). Average OSNR is degraded by 0.5 dB, whereas average Q is reduced by 1.1 dB, which captures OSNR, filter concatenation, and 10-to-10.66-Gb/s rate-increase penalties. Third, for 50% add–drop performed at the sixth OADM, the performance of the pass-through channels (not added/dropped at the sixth OADM) measured after 4160 km and 13 concatenated OADMs is shown by solid triangles in Fig. 16. The performance for the traffic newly added at the sixth OADM (after 1600 km) is also measured after 4160-km transmission and 13 concatenated OADMs (open triangles in Fig. 16). The worst-case Q factor in the 50% add–drop case is more than 2 dB higher than the 7%-FEC threshold for 10^{-15} BER operation. Both pass-through and an added sets of channels in our experimental configuration exhibit the contribution of one crosstalk term. Thus, in agreement with the data in Fig. 14, the Q penalty due to the crosstalk added during the add–drop operation in our OADM system is less than 0.4 dB, owing to the excellent extinction ratio performance of the WB, which performs simultaneous blocking and leveling. In Figs. 15 and 16, we also present the OSNR and Q-factor performance of 10-Gb/s pass-through channels, randomly selected across the WDM spectrum, after 8000 km and 25 concatenated OADMs (solid squares). The measured channels include the channels that have exhibited worst performance at the distance of 4160 km (e.g., channel 69 at 1557.32 nm). At 8000 km, the ASE is the leading impairement, whereas the Q-factor penalty due to crosstalk has been measured to be below 0.2 dB and is not included in the data in Fig. 16. In Fig. 17, we present the measured Q-penalty performance for channel 25 (1539.77 nm) after 13 and 25 OADMs (4160 km and 8000 km, respectively) as a function of frequency detuning of the transmitter around the International Telecommunications Union (ITU) grid. The results capture the effects of FWM crosstalk changes, WB excess-loss-induced OSNR degradation, and WB filter-concatenation-induced spectral clipping. It can be observed that for less than a 0.4-dB overall penalty, the allowable detuning is larger than ± 7 GHz for the case of 13 concatenated WBs and larger than ± 4.5 GHz for the case of 25 concatenated WBs. These measurements represent the worst-case performance due to concatenation of the same WB. The allowable detuning is larger than the accuracy that typical WBs can achieve (± 2.5 GHz), so the WB qualifies for real-life transmitter wavelength offset conditions with a good performance margin.

In the same 80-channel ULH OADM setup, we have also experimentally investigated the feasibility of the dispersion mapping approach proposed in Section III. Fig. 18 shows the Q factor versus propagation distance, measured for channel 25 (1539.77 nm), when no postcompensation is used. With fixed -986 ps/ nm pre-compensation for all channels, optimized for 4160-km transmission distance (52 spans, 28-ps/nm average residual dispersion per span), Q is monotonically decreasing with propagation distance, which ensures the adequate signal performance for any distance shorter than the target 4160-km

TABLE I
SUMMARY OF OSNR AND Q MEASUREMENTS

	Distance, km	OSNR, dB		Q, dB (20 log Q)		Comments
		Minimum	Average	Minimum	Average	
No OADM/OXC	4160	17.1	18.0	15.6	15.8	
OADM, pass-through channels	8000	13.7	14.5	12.2	12.7	no crosstalk
	4160	16.6	17.5	13.7	14.7	no crosstalk
	4160			13.9	14.5	with crosstalk
OADM, added channels	4160			13.6	14.3	with crosstalk
OXC, 40 dB extinction	4160	16.5	17.3	13.5	14.3	best polarization
				13.4	14.2	worst polarization
OXC, 32 dB extinction	4160			12.2	13.6	best polarization
				12.0	13.3	worst polarization

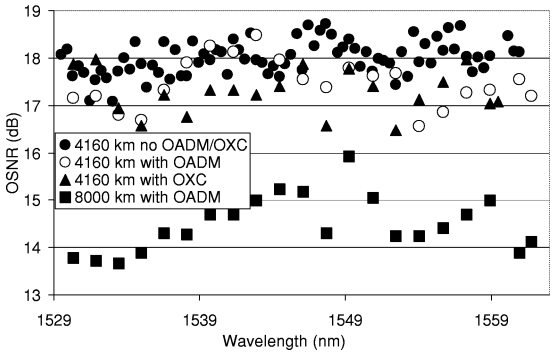

Fig. 15. OSNR after 4160 km and 8000 km.

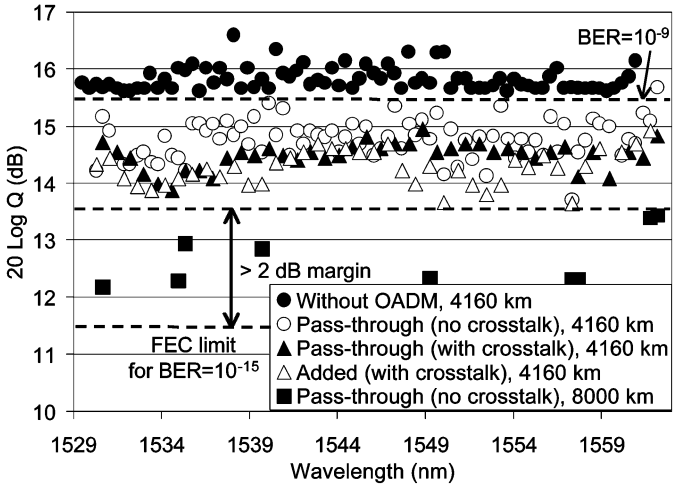

Fig. 16. Q-factor performance of pass-through and added channels after 4160 km, with and without 13 concatenated OADMs, as well as Q factors after 8000 km (25 concatenated OADMs).

value. Even for distances longer than the target, the performance is still better than the FEC threshold at least up to 5120 km (64 spans, 16 OADMs). The dashed line indicates the Q level that could have been achieved if the pre- and postcompensation were reoptimized for every distance measured. This could have provided better performance for a particular target distance but would not guarantee the acceptable Q for the channels dropped at an intermediate location.

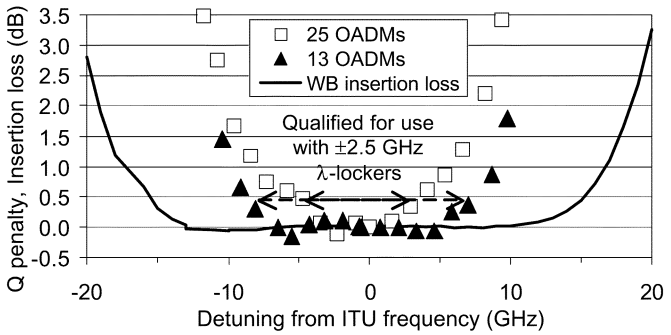

Fig. 17. Q-factor performance for channel 25 (1539.77 nm) as a function of transmitter frequency detuning from the ITU grid; also shown is the WB's insertion loss relative to that at the ITU frequency.

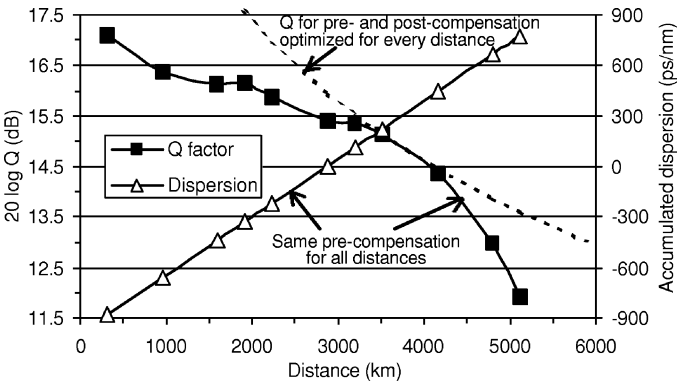

Fig. 18. Q factor and accumulated dispersion versus distance (channel 25, 1539.77 nm).

To summarize this section, we have experimentally realized the dynamically reconfigurable 80×10.66-Gb/s ULH network using a low-loss B&S OADM architecture and characterized the impact of both transmission and networking impairments. We have also demonstrated the feasibility of the dispersion mapping approach of Section III for unregenerated reach distances up to 5120 km.

VIII. 320×320 OXC IN ULTRA-LONG-HAUL NETWORK

This section presents a transport study of the ULH network using reconfigurable B&S OXCs. Similar to the previous section, these experiments are enabled by a WB (Corning®

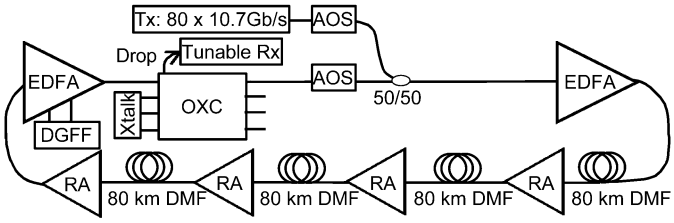

Fig. 19. Experimental setup.

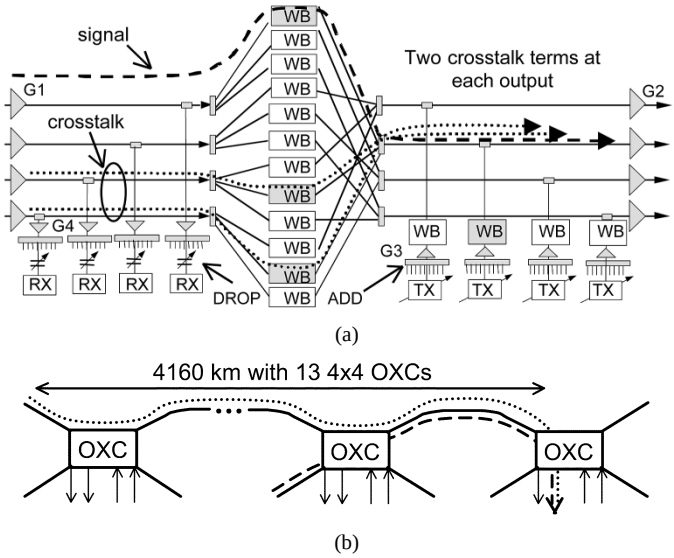

Fig. 20. (a) Our implementation of the B&S OXC architecture. (b) The network model.

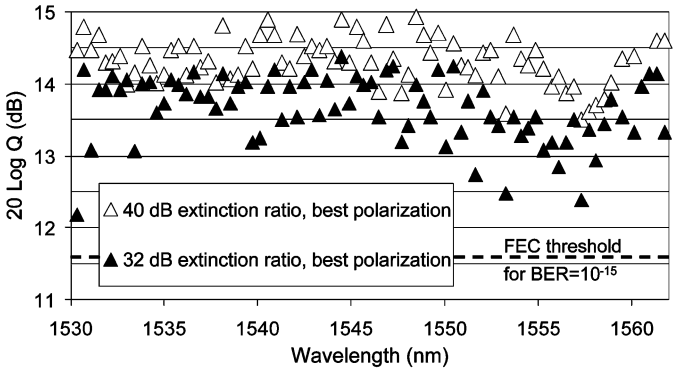

Fig. 21. Q-factor performance after 4160 km and 13 OXCs, best polarization.

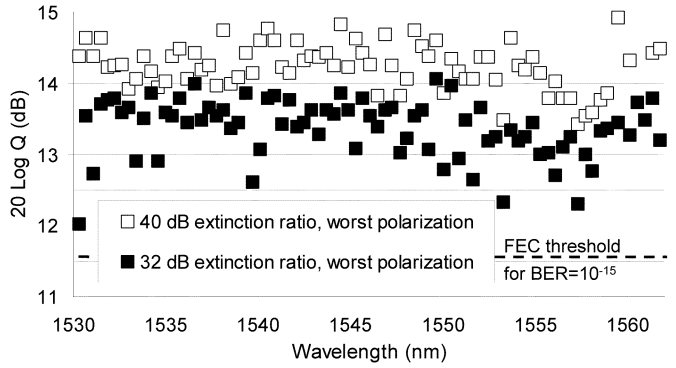

Fig. 22. Q-factor performance after 4160 km and 13 OXCs, worst polarization.

Wavelength Blocker) featuring 40-dB extinction ratio and less than 6-dB insertion loss. While our performance study takes into account both transmission and networking impairments, the crosstalk impairment in the case of OXC can be very significant and becomes the focus of our experiments.

In our experimental setup (Fig. 19), 80 channels are initially loaded through an optical path equivalent to that of the add port of an OXC, except that they travel through a different AOS to enable the loading of the recirculating loop. The 80 channels propagate over 320 km and then enter another OXC where two decorrelated crosstalk signals from other ports of the OXC are added. The signal propagates up to a distance of 4160 km and passes through 13 OXCs where 24 crosstalk terms in total are accumulated.

We use 80 DWDM channels from 1530.33 to 1561.82 nm with 50-GHz spacing. They are NRZ-modulated by $LiNbO_3$ Mach–Zehnder modulators using a $2^{31}-1$ 10.664-Gb/s PRBS data. We employ -986 ps/nm pre-compensation for all channels, with no postcompensation. The pre-emphasis technique discussed in previous sections is utilized here to achieve reasonably uniform OSNR performance (1.5-dB ripple) for all channels after transmission through one loop. After each circulation, the shape of the WDM spectrum is restored by a DGFF placed in the mid-stage of EDFA located at the OXC input port (labeled G1 in Fig. 20). The actual OXC implemented in the laboratory is subequipped by including only four WBs [indicated with the shaded boxes in Fig. 20(a)]. However, the implementation captures exactly the impairments of the full OXC design. All signals go through the top WB that is configured at the minimum loss state. The decorrelated signals are also forwarded to the other ports of the OXC. However, the other two WBs that are connected to the same output port are configured for maximum extinction. Due to the finite extinction ratio, two crosstalk terms will appear at the output port. The transmission line and the inline amplifier settings in the recirculating loop are same as those in two preceding sections. After one loop, the maximum level from the two-crosstalk terms is more than 36 dB below the signal level, while the average WB extinction ratio (single-term crosstalk level) of all channels is about -40 dB. The polarization of the crosstalk signals is varied at the launched point in order to determine the worst and best BER performance. After each loop, new crosstalk terms are added with different polarization states relative to the signal and previously added crosstalk terms. This arrangement is close to a realistic scenario, where the polarization alignments of the signals/crosstalk at the receiver are random.

The OSNR (Fig. 15, solid triangles) and Q factors of all channels (Figs. 21 and 22, open symbols) are measured after 4160 km and 13 concatenated OXCs. By varying the crosstalk polarization state, we capture the best-case (Fig. 21) and the worst-case (Fig. 22) Q performance for every channel. We find that in the case of 13 OXCs along the signal path, there is about a 1.5-dB average Q penalty compared with the point-to-point system of Section VI. The Q penalty due to OSNR reduction only is less than 0.7 dB. Similar to the results from the previous

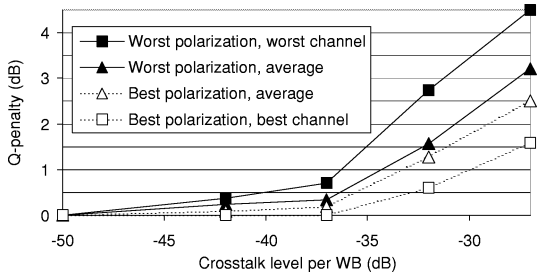

Fig. 23. Q penalty versus crosstalk level per WB (i.e., device extinction ratio). Graph shows the average, best, and worst results among six measured channels.

section, about a 0.4-dB penalty stems from filter concatenation effects. For the received signals after 4160 km, we have measured less than a 0.4-dB Q penalty due to 24 crosstalk terms added by the OXCs. The Q factor for the worst channel is more than 1.8 dB higher than the FEC requirement for 10^{-15} BER. If the average crosstalk performance (extinction ratio) of the WB is artificially reduced to 32 dB, then significant extra penalty ($\sim$ 1 dB) is expected (Figs. 21 and 22, filled symbols). We have also characterized the dependence of the Q penalty due to crosstalk on the average level of crosstalk per WB (Fig. 23). The performance of six channels across the channel plan is measured for various crosstalk levels and for various settings of the polarization-state of the crosstalk signals. The signals and the crosstalk terms for each wavelength experience different evolution of their polarization states as they propagate through the loop. The average, as well as the worst and best Q penalty among the different channels, is measured for each crosstalk level. These results capture, to some extent, the statistical nature of the crosstalk impairment. A crosstalk level per WB of -40 dB results in less than a 0.5-dB penalty, while an implementation with a WB having a -32-dB crosstalk performance may lead to more than a 2.7-dB worst-case penalty. The approximately 1-dB increase in average Q penalty due to a change in WB crosstalk from -40 to -32 dB is in line with the results of Figs. 21 and 22.

Thus, in this section, we have demonstrated the 80×10.66 Gb/s $\times$ 4160 km ULH network using dynamically reconfigurable 320×320 wavelength-port B&S OXCs. The critical issue of the impact of OXC crosstalk has been investigated in detail. We have shown that the WBs with 40-dB extinction ratio provide an adequate crosstalk performance in such a network, whereas the use of 32-dB extinction ratio devices results in considerable penalties.

IX. Summary

Broadcast-and-select OADM and OXC node architectures are promising approaches to next-generation transparent ULH optical networking. We have experimentally demonstrated their excellent suitability for simple cost-effective dispersion management, as well as for minimizing the degradation of the signals passing through such nodes. We have observed the network reach extension benefits of using symmetric dispersion-managed fiber and optimized signal pre-emphasis. Finally, we have experimentally realized the broadcast-and-select OADM and OXC networks with reach in excess of 4000 km, provided detailed characterization of their performance, and proven their robustness with respect to main transmission and network impairments.

References

[1] A. Solheim and J. Frodsham, "Next generation backbone networks," in *Proc. Nat. Fiber Optic Engineers Conf. (NFOEC'01)*, 2001, pp. 1283–1289.

[2] J.-K. Rhee, I. Tomkos, M. Vasilyev, and L. Nederlof, "Ultra-long-haul DWDM network studies with cost-effective reconfigurable OADMs," in *Optical Transmission Systems and Equipment for WDM Networking*, B. Dingle, Ed., 2002, vol. 4872, *Proc. SPIE* (ITCOM'02), pp. 121–128.

[3] A. F. Evans, A. Kobyakov, and M. Vasilyev, "Distributed Raman transmission: Applications and fiber issues," in *Raman Amplifiers for Telecommunications*, M. N. Islam, Ed. New York: Springer-Verlag, 2003, vol. 2.

[4] I. Haxell, N. Robinson, A. Akhtar, M. Ding, and R. Haigh, "2410 km all-optical network field trial with 10 Gb/s DWDM transmission," *Optical Fiber Communication Conf., Tech. Dig.*, pp. PD41-1–PD41-3, 2000.

[5] D. Chen, S. Wheeler, D. Nguyen, B. Davis, M. Glavanovic, J. Khaydarov, I. Koruga, S. Hegarty, F. Cokic, and F. Zhu, "40 channels 4000 km DWDM ULH transmission field trial without Raman amplification and regeneration," *Optical Fiber Communication Conf., Tech. Dig.*, pp. PD FC10-1–FC10-3, 2002.

[6] I. Tomkos, M. Vasilyev, J.-K. Rhee, M. Mehendale, B. Hallock, B. Szalabofka, M. Williams, S. Tsuda, and M. Sharma, "80 $\times$ 10.7 Gb/s ultra-long-haul ($+$4200 km) DWDM network with reconfigurable "broadcast & select" OADM's," *Optical Fiber Communication Conf., Tech. Dig.*, pp. PD FC1-1–FC1-3, 2002.

[7] ——, "Ultra-long-haul DWDM network with 320 $\times$ 320 wavelength-port "broadcast & select" OXC's," in Eur. Conf. Optical Communication, Copenhagen, Denmark, Sept. 2002, Postdeadline Paper PD2.1.

[8] J.-K. Rhee, M.-J. Li, P. Iydroose, M. Zhao, B. Hallock, I. Tomkos, and M. Ajgaonkar, "A novel 240-Gb/s channel-by-channel dedicated optical protection ring network using wavelength selective switches," *Optical Fiber Communication Conf., Tech. Dig.*, pp. PD38-1–PD38-3, 2001.

[9] A. Boskovic, M. Sharma, N. Antoniades, and M. Lee, "Broadcast and select OADM nodes: Application and performance trade-offs," in *OSA Trends Optics Photonics*, vol. 70, Optical Fiber Communication Conf., Tech. Dig., Washington, DC, 2002, pp. 158–159.

[10] M. Vasilyev, B. Szalabofka, S. Tsuda, J. M. Grochocinski, and A. F. Evans, "Reduction of Raman MPI and noise figure in dispersion-managed fiber," *Electron. Lett.*, vol. 38, pp. 271–272, 2002.

[11] S. Bickham, D. Chowdhury, P. Diep, A. Evans, J. M. Grochocinski, P. Han, A. Kobyakov, S. Kumar, G. Luther, J. Mauro, M. Mlejnek, M. Murtagh, M. Muktoyuk, S. Raghavan, V. Ricci, A. Sevian, N. Taylor, S. Tsuda, M. Vasilyev, L. Wang, and Y. Zhu, "Fiber design considerations for 40 Gb/s systems," *J. Lightwave Technol.*, vol. 20, pp. 2290–2305, Dec. 2002.

[12] A. R. Ranalli, B. A. Scott, and J. P. Kondis, "Liquid crystal based wavelength selectable cross-connect," in *Proc. Eur. Conf. Optical Communication*, 1999, pp. 68–69.

[13] P. Bayvel and R. Killey, "Nonlinear optical effects in WDM transmission," in *Optical Fiber Telecommunications IVB*, I. Kaminow and T. Li, Eds. San Diego, CA: Academic, 2002.

[14] A. Ehrhardt, N. Hanik, A. Gladisch, and F. Rumpf, "Field demonstration of a transparent optical 10 Gb/s WDM network based on normalized transmission sections," in *OSA Trends Optics Photonics*, vol. 70, Optical Fiber Communication Conf., Tech. Dig., Washington, DC, 2002, pp. 42–43.

[15] I. Tomkos, M. Vasilyev, J.-K. Rhee, A. Kobyakov, M. Ajgaonkar, and M. Sharma, "Dispersion map design for 10 Gb/s ultra-long-haul DWDM transparent optical networks," presented at the Opto Electronics Communications Conf., Yokohama, Japan, July 2002, PD-1-2.

[16] D. Penninckx, G. Charlet, J.-C. Antona, and L. Noirie, "Experiimental validation of a transparent wave-band-based optical backbone network," presented at the Eur. Conf. Optical Communication, Copenhagen, Denmark, Sept. 2002, 6.4.4.

[17] G. Vareille, B. Julien, F. Pitel, and J. F. Marcerou, "3.65 Tbit/s (365 $\times$ 11.6 Gbit/s) transmission experiment over 6850 km using 22.2 Ghz channel spacing in NRZ format," presented at the Eur. Conf. Optical Communication, Amsterdam, The Netherlands, Sept. 2001, PD.M.1.7.

[18] E. Kollveit, M. O. Berendt, F. A. Annunziata, G. E. Giudice, B. Stevens, and S. Ten, "Temperature independent dispersion managed fiber for 40 Gb/s WDM systems," presented at the Euro. Conf. Optical Communication, Copenhagen, Denmark, Sept. 2002, 5.1.1.
[19] R. Hainberger, T. Hoshida, T. Terahara, and H. Onaka, "Comparison of span configurations of Raman-amplified dispersion-managed fibers," *IEEE Photon. Technol. Lett.*, vol. 14, pp. 471–473, Apr. 2002.
[20] T. Tsuritani, A. Agata, I. Morita, and N. Edagawa, "21.4 Gbit/s × 56 WDM 9170 km transmission using symmetrically dispersion-managed fiber span," *Electron. Lett.*, vol. 37, pp. 1536–1538, 2001.
[21] K. Shimizu, K. Ishida, K. Kinjo, T. Kobayashi, S. Kajiya, T. Tokura, T. Kogure, K. Motoshima, and T. Mizuochi, "65 × 22.8 Gb/s WDM transmission over 8,398 km employing symmetrically collided transmission with A_{eff} management," in *OSA Trends Optics Photonics*, vol. 70, Optical Fiber Communication Conf., Tech. Dig., Washington, DC, 2002, pp. 364–365.
[22] M. Mehendale, M. Vasilyev, A. Kobyakov, M. Williams, and S. Tsuda, "All-Raman transmission of 80 × 10 Gb/s WDM signals with 50 Ghz spacing over 4160 km of dispersion-managed fiber," *Electron. Lett.*, vol. 38, pp. 648–649, 2002.
[23] S. N. Knudsen, B. Zhu, L. E. Nelson, M. Ø. Pederson, D. W. Peckham, and S. Stulz, "420 Gbit/s (42 × 10 Gbit/s) WDM transmission over 4000 km of ultrawave fiber with 100 km dispersion-managed spans and distributed Raman amplification," *Electron. Lett.*, vol. 37, pp. 965–967, 2001.
[24] B. Zhu, L. Leng, L. E. Nelson, S. Knudsen, J. Bromage, D. Peckham, S. Stulz, K. Brar, C. Horn, K. Feder, H. Thiele, and T. Veng, "1.6 Tb/s (40 × 42.7 Gb/s) transmission over 2000 km of fiber with 100-km dispersion-managed spans," presented at the Eur. Conf. Optical Communication, Amsterdam, The Netherlands, Sept. 2001, PD.M.1.8.
[25] F. Liu, J. Bennike, S. Dey, C. Rasmussen, B. Mikkelsen, P. Mamyshev, D. Gapontsev, and V. Ivshin, "1.6 Tbit/s (40 × 42.7 Gb/s) transmission over 3600 km ultrawave fiber with all-Raman amplified 100 km terrestrial spans using ETDM transmitter and receiver," *Optical Fiber Communication Conf., Tech. Dig.*, pp. PD FC7-1–FC7-3, 2002.
[26] A. R. Chraplyvy, J. A. Nagel, and R. W. Tkach, "Equalization in amplified WDM lightwave transmission systems," *IEEE Photon. Technol. Lett.*, vol. 4, pp. 920–922, Aug. 1992.
[27] F. Forghieri, R. W. Tkach, and D. L. Favin, "Simple model of optical amplifier chains to evaluate penalties in WDM systems," *J. Lightwave Technol.*, vol. 16, pp. 1570–1576, Sept. 1998.
[28] O. Tonguz and F. A. Flood, "Gain equalization of EDFA cascades," *J. Lightwave Technol.*, vol. 15, pp. 1832–1841, Oct. 1997.
[29] K. Ennser and V. L. DaSilva, "Impact of optical amplifier gain shape in dense WDM systems," in *Eur. Conf. Optical Communication*, Nice, France, 1999, pp. I-284–I-285.

Michael Vasilyev (S'98–M'99) received the M.Sc. degree in physics from the Moscow Institute of Physics and Technology, Moscow, Russia, in 1993, and the Ph.D. degree in electrical engineering from Northwestern University, Evanston, IL, in 1999.

His research at Lebedev Physics Institute, Moscow, Russia, in 1993–1994 and subsequent doctoral work at Northwestern were on quantum properties of novel optical amplifiers and solitons in optical fibers, including development of homodyne tomography of multimode quantum states and the first experimental demonstrations of noiseless fiber amplifier and noiseless amplification of images. After joining Corning Inc.'s Photonic Research and Test Center, Somerset, NJ, as a Senior Research Scientist in 1999, he performed experimental and theoretical studies of fiber transmission issues, ultra-long-haul DWDM network architectures, and noise and nonlinearities in Raman amplifiers and EDFAs. Since 2003, he has been an Assistant Professor at the Department of Electrical Engineering, University of Texas, Arlington. His research interests include optical communication, quantum and nonlinear optics, and nanophotonics. He has authored and coauthored more than 70 technical papers in journals and conference proceedings.

Dr. Vasilyev is a Member of the IEEE Lasers & Electro-Optics Society (LEOS), the IEEE Communication Society, and the Optical Society of America (OSA), currently serving on the Technical Program Committee for Optical Amplifiers and their Applications (OAA) conference.

Ioannis Tomkos (S'98–A'99–M'02) received the B.S. degree in physics from the University of Patras, Patras, Greece, and the M.Sc. degree in telecommunications engineering and the Ph.D. degree in optical telecommunications from the University of Athens, Athens, Greece, where his Ph.D. work focused on theoretical and experimental studies of novel wavelength conversion technologies based on nonlinear effects in semiconductor optical amplifiers/lasers and fibers.

During his Ph.D. studies, he was a Visiting Researcher in several leading research centers across Europe. In 1996, he joined the Optical Communications Group, University of Athens, where he participated in several national and European research projects (e.g., ACTS and COST) as a Research Fellow. His work there was related to wavelength-division-multiplexing (WDM) technologies for all-optical networks (including characterization of optical components, all-optical signal processing, design of novel optical cross-connects, short-pulse generation, and dispersion compensation) and with digital transmission systems for access networks (e.g., ADSL, HFC technologies). In January 2000, he joined the Photonics Research and Test Center, Corning, Inc., Corning, NY, as a Senior Research Scientist. His research focused in theoretical and experimental studies of transport phenomena related to WDM optical networks. He studied extensively the performance and design issues of metropolitan/regional area optical networks and successfully led several projects. He was then subsequently involved in studies related with transport performance and technology trends in ultra-long-haul optical networks. He has coauthored about 70 contributed and invited papers, published in various international journals and conference proceedings, and he has several patents and patent applications pending.

Dr. Tomkos received educational scholarships from the Hellenic Institute of National Scholarships in 1991–1993. In 1998, he received a grant and also the "Best Student Paper" Award from the IEEE Lasers and Electro-Optics Society (LEOS). In 1999, he received a scholarship from SPIE. In 2000, he was recognized by Corning, Inc., for his contributions in the development of a new optical fiber. In 2002, he received the "2001 Corning Research Outstanding Publication Award." He is a Member of IEEE LEOS and a Member of the Optical Fiber Communication Conference (OFC'03) Committee on "Networks: Switching, Access and Routing." He is also a Reviewer for the JOURNAL OF LIGHTWAVE TECHNOLOGY and the IEEE PHOTONICS TECHNOLOGY LETTERS.

Manjusha Mehendale, photograph and biography not available at the time of publication.

June-Koo Rhee (M'03) received the B.E. and M.Sc. degrees from Seoul National University, Seoul, Korea, in 1988 and 1990, respectively, and the Ph.D. degree from the University of Michigan, Ann Arbor, in 1995, all in electrical engineering.

He gained the postdoctoral experience at Princeton University, Princeton, NJ, as a Research Associate with the Center for Photonics and Opto-Electronic Materials. In 1996, he joined NEC Research Institute, Princeton, as a Scientist in the area of quantum and nonlinear optics study. Since joining Corning, Inc., Corning, NY, in 1998 as a Senior Research Scientist, he has contributed to a broad range of research and development projects in optical network and transmission systems. His present interests are optical network architecture designs and advanced optical modulation formats for ultra-long-haul and metro-area network systems. He has authored and coauthored more than 60 technical papers and conference presentations in the area of optical communications, semiconductor lasers, quantum optics, nonlinear optics, and ultrafast laser science. He is a Peer-Reviewer of *Optics Letters* and *Journal of Optical Society of America B*.

Dr. Rhee is a Peer-Reviewer of IEEE PHOTONICS TECHNOLOGY LETTERS.

Andrey Kobyakov (M'01), photograph and biography not available at the time of publication.

Mahesh Ajgaonkar, photograph and biography not available at the time of publication.

Sergio Tsuda, photograph and biography not available at the time of publication.

Manish Sharma (A'96–M'95), photograph and biography not available at the time of publication.